# nature chemistry

**Article** 

https://doi.org/10.1038/s41557-022-01097-7

# Recyclable cyclic bio-based acrylic polymer via pairwise monomer enchainment by a trifunctional Lewis pair

Received: 24 September 2021

Accepted: 19 October 2022

Published online: 28 November 2022



Yanjiao Song¹, Jianghua He¹, Yuetao Zhang ®¹⊠, Reid A. Gilsdorf ®² & Eugene Y.-X. Chen ®²

The existing catalyst/initiator systems and methodologies used for the synthesis of polymers can access only a few cyclic polymers composed entirely of a single monomer type, and the synthesis of such authentic cyclic polar vinyl polymers (acrylics) devoid of any foreign motifs remains a challenge. Here we report that a tethered B-P-B trifunctional, intramolecular frustrated Lewis pair catalyst enables the synthesis of an authentic cyclic acrylic polymer, cyclic poly(y-methyl-α-methylene-y-butyrolactone) (c-PMMBL), from the bio-based monomer MMBL. Detailed studies have revealed an initiation and propagation mechanism through pairwise monomer enchainment enabled by the cooperative and synergistic initiator/ catalyst sites of the trifunctional catalyst. We propose that macrocyclic intermediates and transition states comprising two catalyst molecules are involved in the catalyst-regulated ring expansion and eventual cyclization, forming authentic c-PMMBL rings and concurrently regenerating the catalyst. The cyclic topology of the c-PMMBL polymers imparts an ~50 °C higher onset decomposition temperature and a much narrower degradation window compared with their linear counterparts of similar molecular weight and dispersity, while maintaining high chemical recyclability.

Cyclic polymers without chain ends are fascinating materials and have continued to capture intense interest<sup>1-5</sup>. Developing more efficient and selective syntheses of diverse cyclic polymer structures will enable reliable material–property evaluations and a better understanding of the effects of their cyclic topology on their physical, mechanical and rheological properties<sup>6-12</sup>, ultimately allowing unique applications of cyclic polymers compared with their linear counterparts<sup>13-19</sup>. However, our knowledge of cyclic polymers is limited due to the difficulty in synthesizing well-defined, diverse classes of cyclic polymers. The current synthetic strategies for synthesizing cyclic polymers can be categorized into two major approaches: ring-closing polymerization (RCP) and ring-expansion polymerization (REP)<sup>3,20</sup>. The RCP strategy through the coupling

of the  $\alpha$ , $\omega$ -terminal functional groups of linear polymer chains unimolecularly or bimolecularly is not limited by monomer type. However, this method often requires multistep functionalization of the linear polymer backbone and high dilution for the ring-closing step. It also affords cyclic polymers with limited molecular weight (MW) $^{21}$ . In contrast, the REP approach can lead to cyclic polymers with high MW under normal or high concentration conditions, but it is limited to a few monomer/polymer classes and requires a specifically designed cyclic catalyst/initiator template system for each monomer class $^{22}$ . Nonetheless, applying the REP strategy to ring-opening olefin metathesis polymerization has enabled the synthesis of high-MW cyclic polymers of cycloalkenes $^1$ , alkynes $^{12,23,24}$  and norbornene $^{25,26}$ . Note that the ring-opening polymerization

¹State Key Laboratory of Supramolecular Structure and Materials, College of Chemistry, Jilin University, Changchun, Jilin, China. ²Department of Chemistry, Colorado State University, Fort Collins, CO, USA. —e-mail: ytzhang2009@jlu.edu.cn

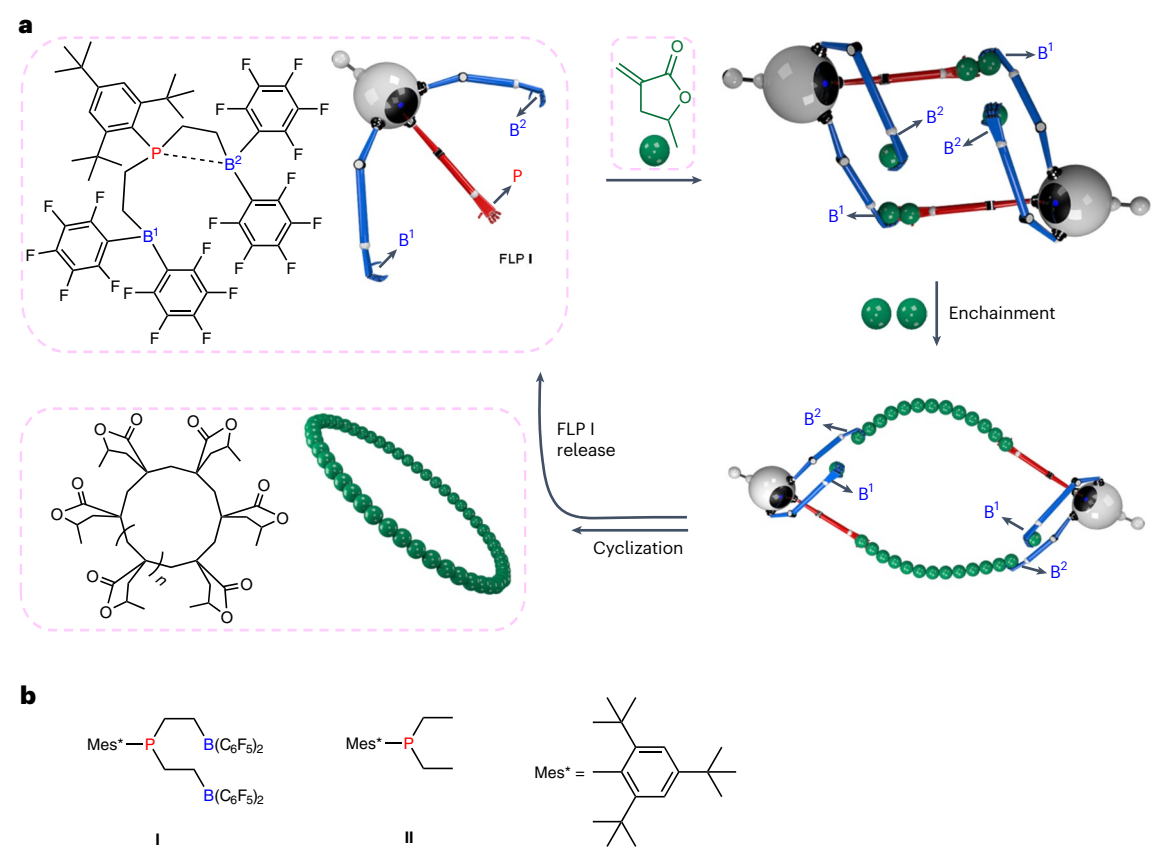


**Fig. 1**| **Hypothesized REP pathway leading to c-PMMBL. a**, Schematic illustration of the formation of c-PMMBL. FLP I reacts with monomer to form a cyclic dimer template, followed by pairwise monomer enchainment for ring expansion and eventual cyclization and regeneration of the catalyst I. The acidic

B sites are coloured blue and labelled B¹ and B², the basic P sites are coloured red and monomers are coloured green. **b**, Structures of tethered trifunctional catalyst B-P-B (**I**) and the monofunctional P control (**II**) used in this work.

(ROP) method is a hybrid strategy that incorporates features of both RCP (through intramolecular cyclization of  $\alpha$ , $\omega$ -chain ends) and REP (through mechanism-dependent, tandem chain propagation and ring closure). The ROP method has enabled the rapid and convenient synthesis of cyclic polymers via either metal-mediated coordination–insertion ROP<sup>2,5,27</sup> or zwitterionic ROP<sup>28–32</sup>.

Since the initial report in 2010<sup>33</sup>, Lewis pair polymerization (LPP) has emerged as a powerful methodology for polymer synthesis<sup>34–37</sup>. In LPP, Lewis acid (LA) and Lewis base (LB) components of Lewis pairs (LPs), particularly frustrated Lewis pairs (FLPs)<sup>38-42</sup>, are used to not only cooperatively and synergistically activate monomers, but also effect chain initiation, propagation and transfer events. It has been successfully implemented to realize the living and controlled polymerization of various polar vinyl monomers<sup>43-47</sup>, ROP<sup>48-55</sup>, as well as for the precision control of monomer sequence<sup>56-58</sup> and polymer topology<sup>28,30,59-62</sup>. Most recently, covalently linked, intramolecular LPs have been shown to exhibit unique synergy and utility in the ROP catalysis of heterocyclic monomers 63-66, but tethered intramolecular LPs had not been reported for vinyl addition polymerization of polar alkenes before this work. We were particularly interested in exploring the potential of such LPs in the synthesis of cyclic polymers of polar vinyl monomers. Previously, Takasu and co-workers reported the synthesis of cyclic poly(alkyl sorbate) from methyl (E,E)-sorbate with an intermolecular LP consisting of the LA bis(2,6-di-tert-butyl-4-methylphenoxy)methylaluminium and the LB 1,3-di-tert-butylimidazolin-2-ylidene<sup>60</sup>. This sorbate/LP system was later used by Takasu and co-workers<sup>61</sup> to synthesize cyclic poly(methyl methacrylate) (PMMA) and by Chen and co-workers<sup>59</sup>

to synthesize cyclic block copolymers of highly reactive acrylates. However, in this method, the introduction of stoichiometric sorbate monomer at the  $\alpha$ -terminus of the polymer chain (for ring closure via nucleophilic cyclization) and the unique structure of sorbate monomers/co-initiators are both requisites for cyclic polymer formation, affording cyclic acrylic polymers bearing the sorbate unit. To address the challenge of synthesizing authentic cyclic acrylic polymers devoid of other non-parent monomer units, we hypothesized that a covalently tethered B-P-B trifunctional FLP catalyst/initiator, such as FLPI (Fig. 1b) 67,68 composed of two acidic B sites and one basic P site that naturally satisfy the required 2:1 LA/LB ratio based on the LPP mechanism (that is, one LA activates the monomer while the other stabilizes the active chain end)<sup>69</sup>, could afford authentic cyclic acrylic polymer chains. In the postulated overall pathway outlined in Fig. 1, FLP I reacts with monomer to form a cyclic dimer template that establishes the basis for subsequent LP-regulated REP via pairwise monomer enchainment, with eventual cyclization leading to authentic acrylic polymer rings and regeneration of the the catalyst I. In this work, we chose γ-methyl-α-methylene-γ-butyrolactone (MMBL) because it not only is bio-based but also leads to the corresponding polymer PMMBL, which exhibits performance-enhanced properties compared with its petroleum-based PMMA counterpart<sup>70-72</sup>. In addition, PMMBL, despite its greater thermal stability and better performance compared with PMMA, was recently shown to be chemically more recyclable, leading to the recovery of pure monomer in a considerably higher yield due to the lactone-imparted stability of the macroradicals generated in the random chain scission processes of thermolysis<sup>73</sup>.

## **Results and discussion**

#### Formation and characterization of c-PMMBL

As shown in Fig. 2a, with a FLP catalyst loading of 0.25%, full monomer consumption was achieved within 14 min. Changing the [MMBL] $_0$ /[I] $_0$  ratio from 100:1 to 200:1 and 400:1 increased the number-averaged molecular mass ( $M_n$ ) of the resulting PMMBL from 232 to 316 and 344 kg mol $^{-1}$ , respectively (Fig. 2a, entries 1–3). The dispersity of the polymers was found to be relatively broad ( $\theta$  = 1.50–1.61), indicative of a non-living polymerization process and a sign of chain transfer events (vide infra) $^1$ . Further increasing the [MMBL] $_0$ /[I] $_0$  ratio to 800:1 and 1,200:1 enhanced the PMMBL  $M_n$  to 383 and 403 kg mol $^{-1}$ , respectively (Fig. 2a, entries 4 and 5), but not proportionally to the monomer-to-catalyst/initiator ratio, further indicating that other processes such as chain transfer compete with chain growth.

To identify the chain initiation and termination end groups of the resulting polymers, we analysed a low-MW oligomeric PMMBL sample produced with trifunctional FLP I by matrix-assisted laser desorption/ionization time-of-flight mass spectroscopy (MALDI-TOF MS). The mass spectrum in Fig. 2b shows two series of molecular ions, which, at first glance, seems to indicate the presence of two different chain initiation/termination pathways giving two different types of chain. Plotting the m/z values for the major and minor series in the MS spectrum versus the number of 2MMBL repeat units afforded the relationships  $y_1 = 224.12x + 135.15$  (Fig. 2c) and  $y_2 = 224.13x + 23.07$ (Fig. 2d), corresponding to the structures [ $(2MMBL)_n + MMBL + Na^+$ ] and  $[(2MMBL)_n + Na^+]$ , respectively. The results of this analysis indicate that two MMBL molecules are required for each monomer enchainment cycle, no matter which m/z series (major or minor). Furthermore, the fact that no end groups were detected for either series suggests the formation of cyclic polymers, and the m/z difference of 112 (that is, a MMBL unit) between the two series points to cyclized rings with an even and odd number of MMBL units (vide infra). To further validate the cyclic topology of the resulting PMMBL, we compared the intrinsic viscosities of the PMMBL produced with FLP  $I([\eta]_t)$  and a known linear PMMBL (I-PMMBL) prepared with an FLP consisting of an imidazolin -2-ylideneaminophosphine (IAP) and Al( $C_6F_5$ )<sub>3</sub> ( $[\eta]_{linear}$ )<sup>47</sup>. As shown in the Mark-Houwink plot (Fig. 2e), as expected,  $[\eta]_I$  is less than  $[\eta]_{linear}$ , with  $[\eta]_{I}/[\eta]_{linear} \approx 0.7$ , thereby confirming the cyclic topology of the PMMBL produced with FLP I.

To probe the applicability of trifunctional FLP I for the polymerization of different monomers to cyclic polymers and to post-functionalize the polymers, we used I to polymerize 3-methylene-5 -vinyldihydrofuran-2(3H)-one (VMBL), which can be readily polymerized by I and contains an unconjugated vinyl functional group suitable for post-modification. VMBL was randomly copolymerized with MMBL in the presence of FLP I (MMBL/VMBL/I = 50:50:1), reaching quantitative monomer conversion in 3 h. <sup>1</sup>H NMR spectroscopy revealed that the produced PMMBL-ran-PVMBL possessed a 1:1 MMBL/VMBL ratio, and gel permeation chromatography (GPC) traces revealed the unimodal MW distribution of the polymer (Supplementary Fig. 30). Using the vinyl groups of the VMBL units retained in the polymer chain, we post-functionalized c-PMMBL<sub>50</sub>-ran-PVMBL<sub>50</sub> by thiol-ene click reaction using poly(ethylene glycol) methyl ether thiol (MPEG2000-SH,  $M_{\rm n}$  = 2,000) to successfully obtain the PEG2000-grafted cyclic copolymer c-PMMBL<sub>50</sub>-ran-PVMBL<sub>50</sub>-g-PEG2000 (Supplementary Fig. 31). Although only around 50% of the vinyl groups of the copolymer were consumed due to the high MW of MPEG2000-SH, a transmission electron microscopy (TEM) image of the grafted copolymer clearly

displayed the anticipated ring structure with diameters of 30–40 nm (Fig. 2f), which further confirmed the formation of the cyclic polymer by this strategy.

#### Characterization of cyclic active species (templates for REP)

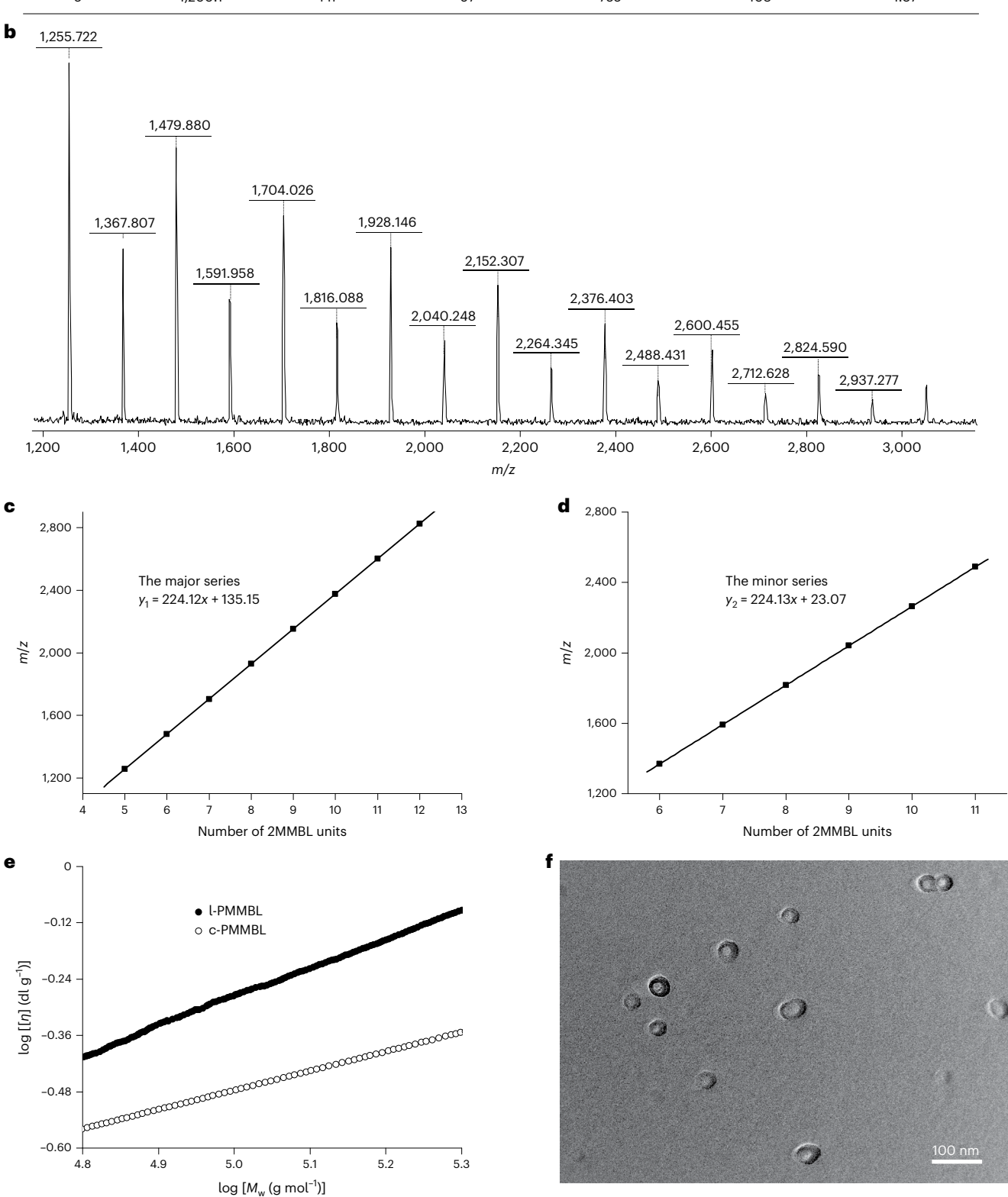
The above results showed that the trifunctional, tethered B-P-B I uniquely produced c-PMMBL, prompting us to seek mechanistic insights into this unusual polymerization system. In this context, the stoichiometric reaction of FLP I with MMBL produced cyclic bimolecular product **1A** and cyclic unimolecular product **1B** in an approximately equimolar ratio (Fig. 3a and Supplementary Fig. 5). Following further purification, 1A was isolated and structurally characterized (Supplementary Figs. 8-14). As shown in the <sup>1</sup>H-<sup>13</sup>C heteronuclear single quantum coherence (HSOC: Supplementary Fig. 11) and <sup>1</sup>H-<sup>1</sup>H correlation spectroscopy (COSY; Supplementary Fig. 12) spectra of 1A, the peaks at 1.35 and -0.53 ppm in the <sup>1</sup>H NMR spectra correlate with the <sup>1</sup>H signal at 2.45 ppm (-PCH<sub>2</sub>-), and thus can be assigned to protons from the same -CH<sub>2</sub>B- group. Noteworthy here is the observation of only one pair of diastereomers (out of four possible pairs) of the cyclic bimolecular product 1A, indicating that the reaction of FLP I and MMBL is diastereoselective. Single-crystal X-ray diffraction analysis of 1A (Fig. 3b and Supplementary Table 1) revealed that it consists of two I and two MMBL molecules, a cyclic bimolecular structure that acts as the starting cyclic template for the ensuing REP process. In this cyclic structure, the P atom and one B atom of one FLP I are separately attached to the C=C bond of one MMBL through 1,2-P,B addition, while the other B atom is coordinated to the carbonyl oxygen of the other MMBL. The other FLP Ladopts the same coordination pattern such that a 16-membered macrocycle is formed from two I molecules and two MMBL molecules. which is a drastically different structure from the previously reported enolate adducts generated from the reactions of intermolecular LPs and monomers 47,74,75. It should be noted that the length of the B2-C20 bond (1.733 Å), which can be thought of a C-bonded enolate motif, is significantly longer than that of a typical B-C single bond (~1.65 Å) and thus more susceptible to cleavage under suitable conditions (for example, in the presence of excess monomer in polymerization reactions). In contrast, the length of the B1–O2 coordination bond (1.579 Å), which can be thought of as an O-bonded enolate motif, is close to that of a normal B-O coordination bond (1.54 Å). Therefore, compared with the B1-O2 bond (O-bonded enolate), it would be easier for the B2-C20 bond (C-bonded enolate) to be broken. This analysis suggests that the B2 centre can be considered as the active LA site to grab a free MMBL molecule from solution and activate it for the subsequent propagation reaction. Overall, such important structural information provides critical insights into a fundamental understanding of the templated REP of MMBL to c-PMMBL via the proposed unusual pairwise monomer enchainment.

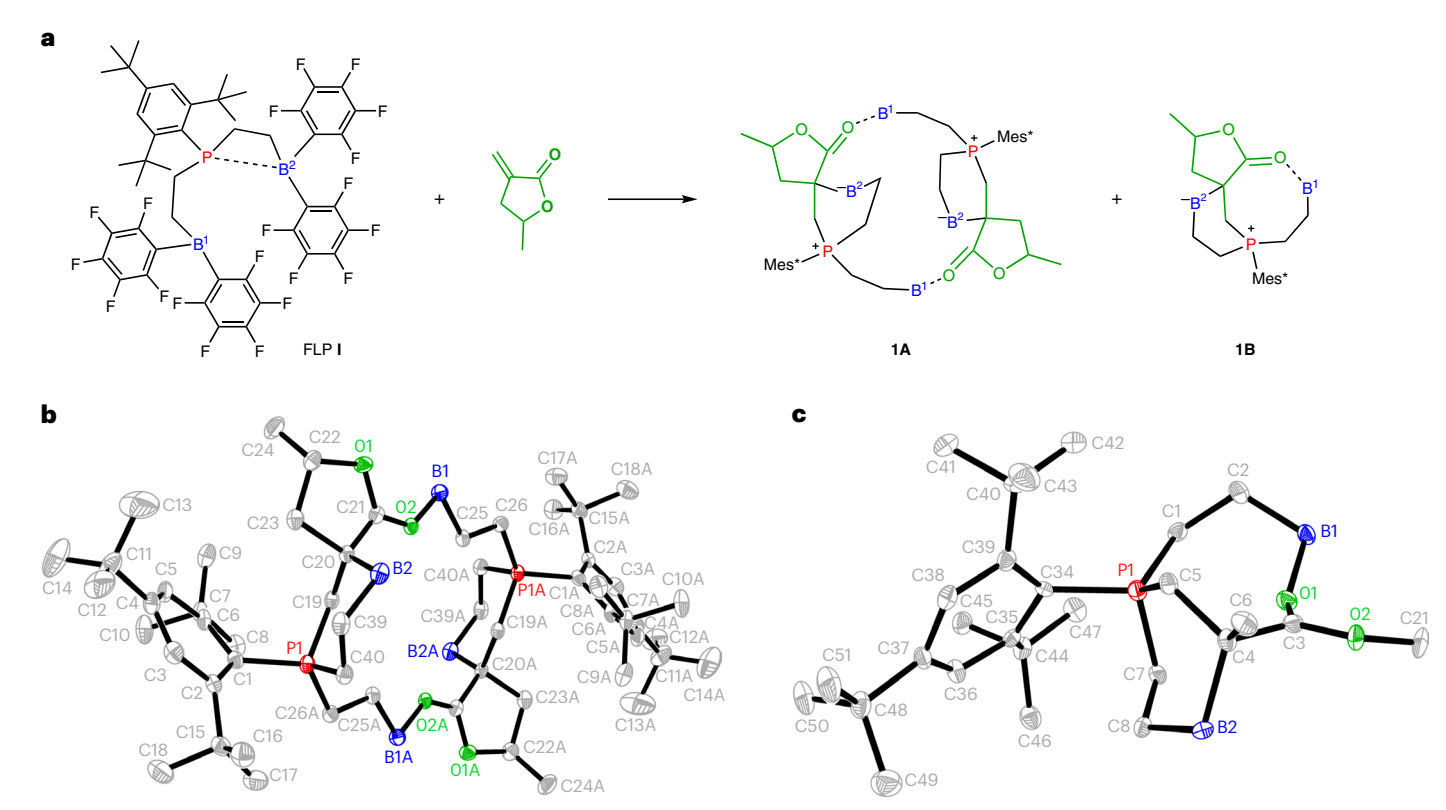
Attempts to obtain the single-crystal X-ray structure of  ${\bf 1B}$  were unsuccessful. Based on its NMR spectroscopic data (Supplementary Fig. 5),  ${\bf 1B}$  should have a structure similar to that of  ${\bf 1A}$ . For example, the peak at -0.53 ppm for  ${\bf 1A}$  and at -0.69 ppm for  ${\bf 1B}$  can be attributed to one proton of the -CH<sub>2</sub>B- group, while the resonance at 5.21 ppm for  ${\bf 1A}$  and at 4.96 ppm for  ${\bf 1B}$  can be assigned to the methine groups of MMBL. Based on the whole analysis described above,  ${\bf 1B}$  is proposed to contain one FLP  ${\bf I}$  and one MMBL monomer, namely it is a unimolecular cycle. This assignment was further confirmed by the exclusive generation of cyclic unimolecular intermediate  ${\bf 2}$  from the reaction of linear analogue methyl methacrylate (MMA)

**Fig. 2** | **Characterization of polymer topology. a**, Table showing selected polymerization data for PMMBL prepared from MMBL with FLP I in dichloromethane at room temperature (-25 °C) with [M] $_0$  = 0.936 M. <sup>a</sup>Monomer conversion was measured by <sup>1</sup>H NMR spectroscopy. <sup>b</sup>Absolute weight-averaged molecular mass ( $M_w$ ) was measured by GPC using a light scattering detector. <sup>c</sup> $M_n$  was calculated from  $M_w/D$ . <sup>d</sup> $D = M_w/M_n$ . **b**, MALDI-TOF MS spectrum of MMBL

oligomers produced with FLP **I. c,d**, Plots of m/z versus the number of 2MMBL repeat units for the major  $(\mathbf{c})$  and minor  $(\mathbf{d})$  series of molecular ions in  $\mathbf{b}$ .  $\mathbf{e}$ , Comparison of the intrinsic viscosity of I-PMMBL and c-PMMBL, reported as Mark–Houwink plots for I-PMMBL produced with IAP–AI( $C_6F_5$ )<sub>3</sub> and c-PMMBL produced with **I. f**, TEM image of c-PMMBL<sub>50</sub>-ran-PVMBL<sub>50</sub>-g-PEG2000.

<b>a</b> -							
٠.	Entry	[M]/[ <b>I</b> ]	Time	Conversion <sup>a</sup> (%)	$M_{\rm w}^{\ \ b}$ (kg mol <sup>-1</sup> )	$M_{\rm n}^{\rm c}$ (kg mol <sup>-1</sup> )	Ð <sup>d</sup>
	1	100:1	10 min	100	348	232	1.50
	2	200:1	10 min	100	508	316	1.61
	3	400:1	14 min	100	544	344	1.58
	4	800:1	2 h	>99	735	383	1.92
	5	1,200:1	4 h	97	755	403	1.87





 $\label{eq:Fig.3} Isolation and structural characterization of reactive intermediates. a, Reaction of FLP I with MMBL affords cyclic bimolecular and unimolecular intermediates <math>{\bf 1A}$  and  ${\bf 1B}$ , respectively. The two B atoms are designated  ${\bf B}^1$  and  ${\bf B}^2$  for clarity.  ${\bf b}$ , X-ray crystal structure of cyclic bimolecular intermediate  ${\bf 1A}$ .  ${\bf c}$ , X-ray crystal structure of cyclic unimolecular intermediate  ${\bf 2C}$  (generated from the reaction of FLP I and MMA), which is a model for cyclic unimolecular  ${\bf 1B}$ . All the

hydrogen atoms and  $C_6F_s$  groups on B have been omitted for clarity and ellipsoids are drawn at the 30% probability level. In the chemical structures in  $\mathbf a$ , the B sites are coloured blue, the P sites are coloured red, and the monomer and parts of the intermediates derived from the monomer are coloured green. The same colour coding is used in the X-ray structures in  $\mathbf b$  and  $\mathbf c$ . The O atoms of monomers are coloured green to distinguish them from C atoms, which are shown in grey.

and FLP I (Supplementary Figs. 17–22). Cyclic 2 also exhibited a characteristic peak at -0.66 ppm, attributed to one proton of -CH<sub>2</sub>B-(Supplementary Fig. 18), and correlations with the proton signal at 1.12 ppm attributed to the other H of the same -CH<sub>2</sub>B- and one proton attributed to the -PCH<sub>2</sub>- group, as shown in its <sup>1</sup>H-<sup>1</sup>H COSY spectrum (Supplementary Fig. 19). The X-ray crystal structure of 2 showed that it is composed of one LP molecule and one MMA molecule, in which P and B atoms of FLP I have added to the C=C double bond of MMA through 1,2-P,B addition, respectively (Fig. 3c). These combined results verify the structure of 1B, even though its structure could not be identified directly. Furthermore, we monitored the conversion of **1A** into **1B** on heating a solution of **1A** at 90 °C and found that the amount of **1B** slowly increased with a decrease in **1A**, reaching 73% after 29 h (Supplementary Fig. 15). The conversion rate was significantly accelerated using fluorobenzene instead of [2H2]dichloromethane as solvent, requiring only 2.67 h to reach a comparable conversion of 1A (Supplementary Fig. 16).

As a control experiment, we analysed the low-MW oligomeric PMMBL sample produced by a mixture of  $\mathbf{1A}$  and  $\mathbf{1B}$ . Two series of molecular mass ions were observed in the MALDI-TOF mass spectrum corresponding to the structures of  $[(2MMBL)_n + MMBL + K^*]$  and  $[(2MMBL)_n + K^*]$ , respectively (Supplementary Fig. 25). Based on the above results, we can draw the same conclusion that two MMBL molecules are required for each enchainment and that no FLP molecule or fragment is attached to the polymer chain. Thus, the polymer obtained from the mixture of  $\mathbf{1A}$  and  $\mathbf{1B}$  is exactly the same as that obtained with FLP  $\mathbf{I}$ , thus demonstrating that  $\mathbf{1A}$  and  $\mathbf{1B}$  are the active intermediates in the polymerization of MMBL starting with FLP  $\mathbf{I}$  and that they produce the same polymer structure.

#### Polymerization kinetics and kinetic scenarios

Next, we investigated how these cyclic active species relate to the chain propagation by conducting kinetics studies of MMBL polymerization mediated by pure 1A and a mixture of 1A and 1B. Both catalyst systems clearly showed a zero-order dependence on [MMBL] concentration for all [MMBL]/[P]<sub>total</sub> ratios investigated ([P]<sub>total</sub>, the concentration of all P sites in the catalyst system, Fig. 4a,b), as similarly reported for LPP catalysed by intermolecular LPs<sup>44,58,69,74</sup>. These results indicated that, in this intramolecular, trifunctional FLP system, the monomer needs to be coordinated to, and activated by, the LA before enchainment via nucleophilic attack by the propagating chain end, and therefore the rate-determining step (RDS) is not related to the free monomer concentration. Based on the structural information of 1A and 1B and the mechanism proposed for LPP with intermolecular LPs, we proposed two kinds of ground state (the unimolecular state, denoted as monomeric M, and bimolecular state, denoted as dimeric **D**) and their corresponding transition states for monomer enchainment (Fig. 4c). Along the dimeric cycle pathway, cleavage of the B<sup>2</sup>-C (C-bonded enolate in **1A**) bond by the incoming monomer generates dimeric cycle **D** with two activated MMBL molecules, and the RDS involves the nucleophilic attack of the B<sup>2</sup>-activated monomer by the zwitterionic enolate species. The monomer coordination/activation step for the monomeric pathway is thought to be the same as above, but the subsequent propagation step is proposed to be different, based on the results of the polymerization kinetics study. Specifically, a double logarithmic plot of the apparent rate constants ( $k_{app}$ ), obtained from the slopes of the best-fit lines to the plots of [MMBL]<sub>0</sub>/[MMBL]<sub>0</sub> versus time, as a function of the concentration of all P sites ([P]<sub>total</sub>) was fitted to a straight

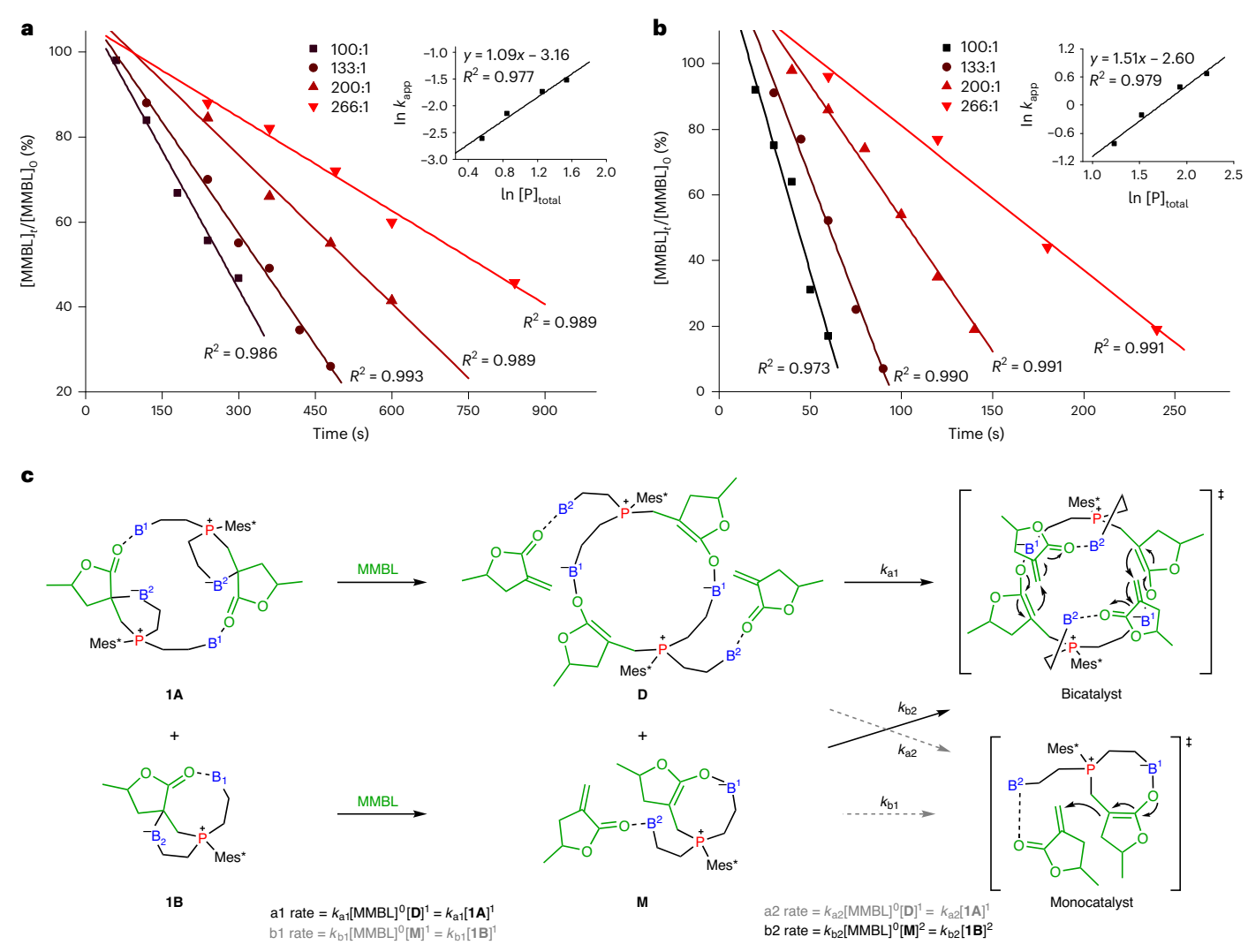


**Fig. 4** | **Polymerization kinetics and possible kinetic scenarios for MMBL polymerization. a,b**, Zero-order kinetic plots for MMBL polymerization using  ${\bf 1A}$  ( ${\bf a}$ ) and a mixture of  ${\bf 1A}$  and  ${\bf 1B}$  ( ${\bf b}$ ) in dichloromethane at room temperature. Insets: plots of  ${\bf In}$   $k_{\rm app}$  versus  ${\bf In}$  [P] $_{\rm total}$  extracted from two sets of polymerization kinetics. [P] $_{\rm total}$  =  $2 \times [{\bf 1A}] + [{\bf 1B}]$ , representing the total concentration of P sites in the system.  ${\bf c}$ , Fundamental steps from the starting bimolecular cycle  ${\bf 1A}$  and

unimolecular cycle  ${f 1B}$  templates to catalyst–monomer complexes  ${f D}$  and  ${f M}$ , respectively, and their corresponding transition states for monomer enchainment. The corresponding kinetic equations for the proposed RDSs with  ${f 1A}$  and  ${f 1B}$  are also shown. In the chemical structures in  ${f c}$ , the B sites (designated  ${f B}^1$  and  ${f B}^2$  for clarity) are coloured blue, the P sites are coloured red, and the monomer and parts of the intermediates derived from the monomer are coloured green.

line ( $R^2 = 0.977$ ) with a slope of 1.1 (Fig. 4a, inset), revealing that the propagation has a first-order dependence on the concentration of **1A.** For the monomeric cycle **M** derived from **1B**, if a monocatalyst transition state is adopted ( $k_{h1}$  route), in principle, the propagation should have a first-order dependence on [M], such that the kinetic order of the the reaction of a mixture of 1A and 1B would be 1 (for both  $k_{\rm al}$  and  $k_{\rm bl}$  routes). Conversely, if a bicatalyst transition state is followed ( $k_{b2}$  route), the propagation should have a second-order dependence on [M], such that the kinetic order of the reaction with a mixture of 1A and 1B would be between 1 and 2. In practice, as revealed by the inset in Fig. 4b, the kinetic order obtained for the mixture of 1A and 1B is 1.5 (between 1 and 2). Therefore it can be concluded that monomeric cycle M also reacts via the bicatalyst transition state (that is, the  $k_{\rm h2}$  route). Furthermore, kinetic studies were conducted for the polymerization of MMBL catalysed by FLP I, which also revealed a zero-order dependence on monomer concentration and a kinetic order of 1.62 for FLP I ( $R^2 = 0.999$ ; Supplementary Fig. 24). These results are similar to those obtained with the mixture of 1A and 1B, thus confirming that both dimeric and monomeric cycles 1A and 1B are active species for propagating polymer chains via the proposed bicatalyst transition state ( $k_{a1}$  and  $k_{b2}$  routes, Fig. 4c).

# Mechanism of c-PMMBL formation

On the basis of the above-described experimental details, structural characterizations of active species, and polymerization and kinetic studies, we can propose an overall mechanism for the formation of c-PMMBL rendered by trifunctional B-P-B I (Fig. 5). In the first step, the reaction of FLP I with MMBL affords bimolecular cycle 1A and unimolecular cycle 1B for the ensuing REP. Both cyclic templates have been shown to be kinetically competent for polymerization, which proceeds through the same postulated bicatalyst transition state, formed by cleavage of the labile  $B^2$ –C (C-bonded enolate) bond by the incoming MMBL to generate the activated catalyst–monomer complex. Subsequent Michael addition to the activated monomer by the active enolate chain end connected to the O-bonded  $B^1$  results in the insertion of one monomer into the growing polymer chain. Meanwhile,  $B^1$  is released from the polymer chain and swaps roles with  $B^2$  to activate another incoming monomer in the next monomer addition cycle, followed

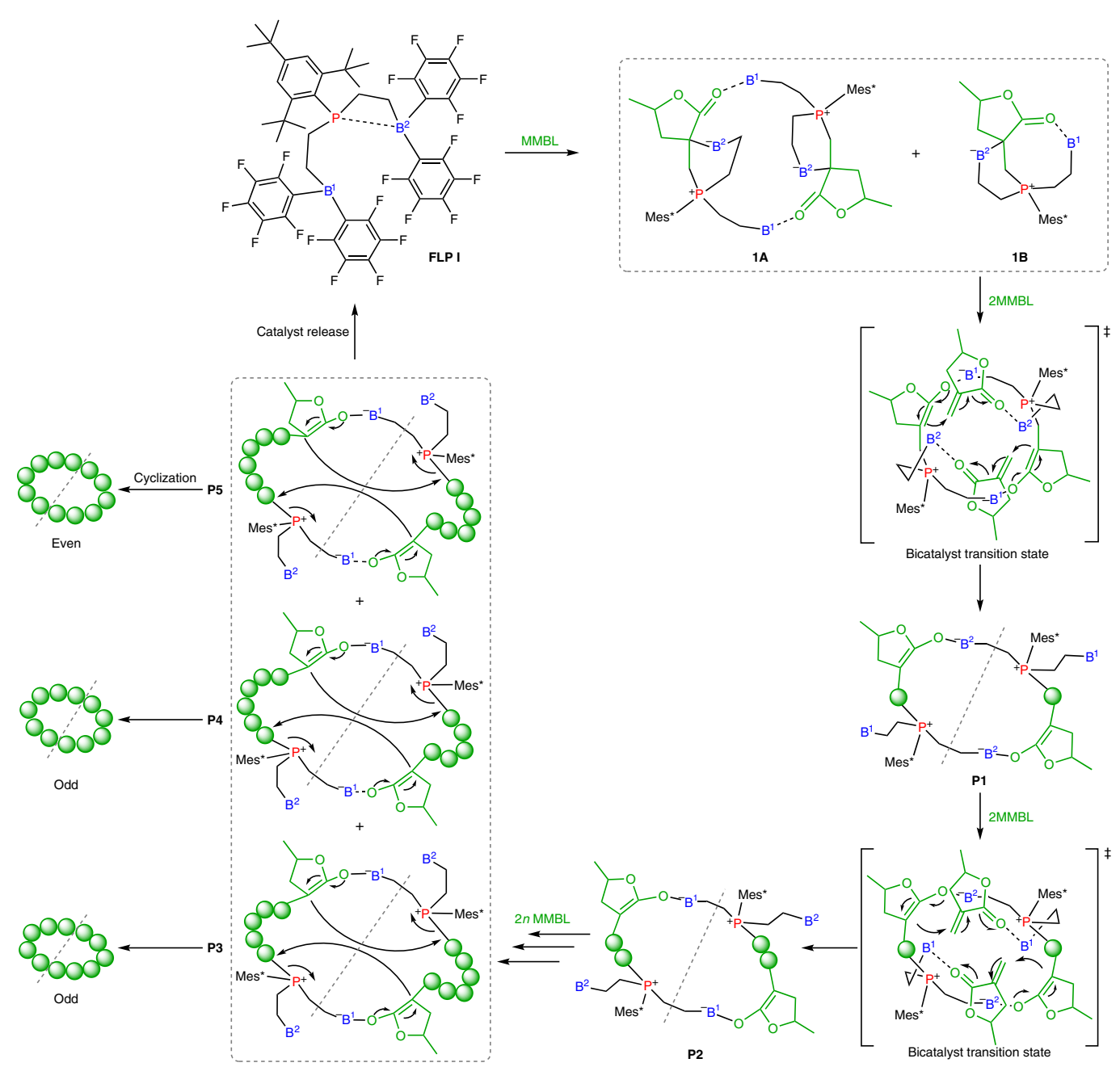


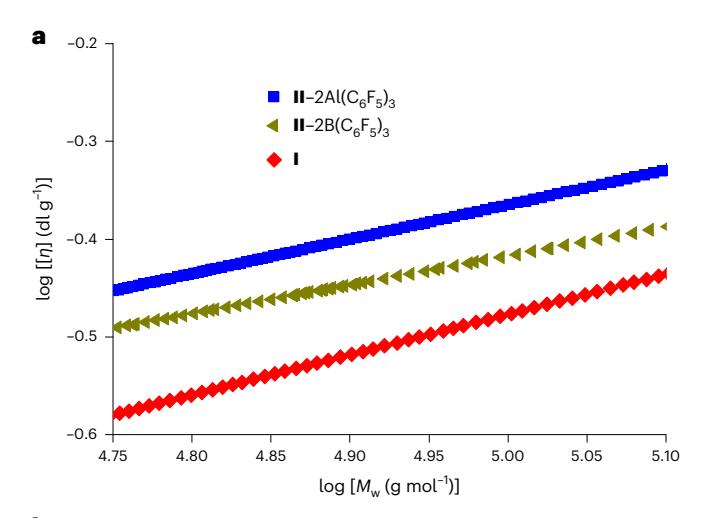
**Fig. 5** | **Proposed REP mechanism for creating c-PMMBL.** The key fundamental steps in the synthesis of c-PMMBL, including the formation of the cyclic templates **1A** and **1B** through 1,2-P,B addition of the catalyst to MMBL with the same stoichiometry, subsequent monomer coordination/activation and insertion events in the cyclic templates **1A** and **1B** and the bicatalyst transition state, ring expansion by concurrent repeated pairwise monomer enchainment at

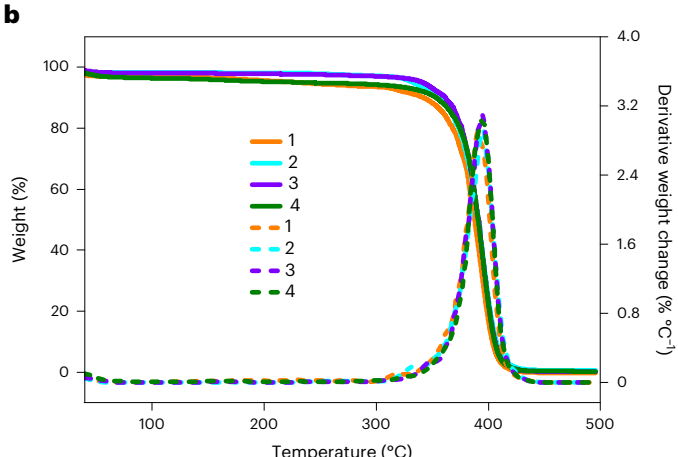
the two LP catalyst sites in the bicatalyst transition state and ring closure to yield cyclic polymers with odd- and even-numbered MMBL units and regenerate the catalyst. The B sites (designated  $B^1$  and  $B^2$  for clarity) are coloured blue, the P sites are coloured red, and the monomer and parts of the intermediates derived from the monomer are coloured green, with green circles representing the MMBL monomer. The two  $C_6F_5$  groups on each B have been omitted for clarity.

by Michael addition of the active enolate chain end connected to  $B^2$ . Through this repeated monomer activation and addition assisted by the alternating roles of the  $B^1$  and  $B^2$  sites, monomer is continuously incorporated into the growing polymer chain and the ring keeps expanding (thus REP). As the polymerization proceeds through a bicatalyst transition state, a pair of monomer molecules can be inserted concurrently into the polymer chains grown from the two LP sites, thus achieving unique pairwise monomer enchainment in this REP.

On completion of polymerization, the trifunctional LPs would have a P atom linked to the  $\alpha$ -terminus of one polymer chain and a B atom connected to the  $\omega$ -terminus of the other polymer chain (Fig. 5).

Through this connectivity, the two concurrently growing polymer chains are kept in close proximity, which promotes cyclization via nucleophilic attack of the  $\alpha$ -terminus of one chain by the  $\omega$ -terminus (nucleophilic enolate) of the other chain, resulting in ring closure to form c-PMMBL with concurrent release of the LP catalysts from the chains. This mechanism also explains the cyclic structures formed with both odd- and even-numbered monomer units revealed by MALDI-TOF MS. Specifically, here we use the term 'pairwise monomer enchainment' to indicate that two monomers can be enchained at once due to the presence of the two catalyst sites in the bicatalyst REP template, but it does not necessarily mean that the two sites would have





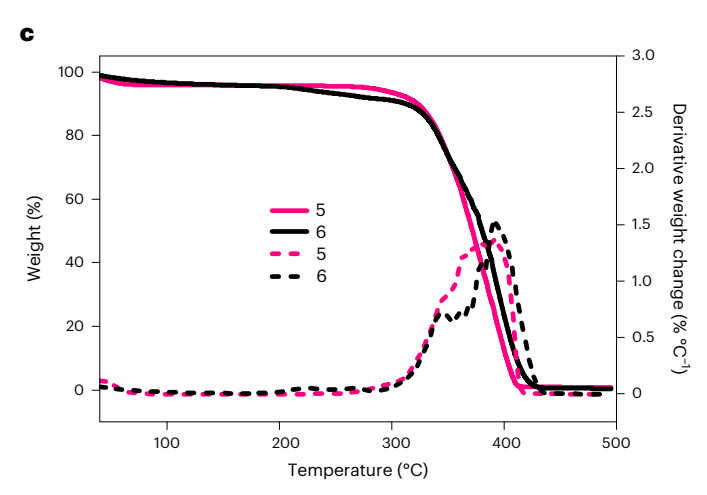


**Fig. 6** | **Comparison of the properties of PMMBL with different topologies. a**, Comparison of the intrinsic viscosity of PMMBLs with different topologies, reported as Mark–Houwink plots: c-PMMBL produced by FLP **I**, a mixture of cyclic and linear PMMBLs produced by intermolecular **II**–2B( $C_6F_5$ )<sub>3</sub> and l-PMMBL produced by intermolecular LP **II**–2Al( $C_6F_5$ )<sub>3</sub>. **b**, Overlay of TGA (solid lines) and DTG (dashed lines) curves for c-PMMBL samples with four different MWs: sample 1,  $M_n$  = 93.1 kg mol<sup>-1</sup>, D = 1.31; sample 2,  $M_n$  = 109 kg mol<sup>-1</sup>, D = 1.21; sample 3,  $M_n$  = 176 kg mol<sup>-1</sup>, D = 1.41; sample 4,  $M_n$  = 403 kg mol<sup>-1</sup>, D = 1.88. **c**, Overlay of TGA (solid lines) and DTG (dashed lines) curves for l-PMMBL samples with two different MWs: sample 5,  $M_n$  = 289 kg mol<sup>-1</sup>, D = 1.82; sample 6,  $M_n$  = 427 kg mol<sup>-1</sup>, D = 1.77.

identical propagation rates. Thus, three propagation-cyclization scenarios can be envisioned (Fig. 5): (1) an equal number of monomers are added to the polymer chain on each side of the dotted line

dividing the macrocycle (**P5**), (2) one more monomer is added to the chain on the left side than to the chain on the right side (**P4**) and (3) one more monomer is added to the chain on the right side than to the chain on the left side (**P3**). Therefore the probability for the formation of odd-numbered MMBL units (**P3** + **P4**) is higher than that for the formation of even-numbered MMBL units (**P5**), which is consistent with our MALDI-TOF MS analysis, which revealed that the ratio of the major series, attributed to the odd-numbered c-PMMBL, to the minor series, attributed to the even-numbered c-PMMBL, is approximately 1.7 (Fig. 2b).

To determine whether the trifunctionality of the intramolecular B-P-B FLP I is a requisite for the selective production of c-PMMBL, we synthesized a monofunctional compound without the Lewis acidic B site, namely Mes\*P(CH<sub>2</sub>CH<sub>2</sub>)<sub>2</sub>(II, Fig.1b), which serves only as a LB, for a comparative study. MALDI-TOF MS of the oligomeric PMMBL produced using the intermolecular LP II –  $2Al(C_6F_5)_3$  showed the formation of the linear structure with the α-terminus capped by LB II (Supplementary Fig. 27). Interestingly, the combination of LB II and B( $C_6F_5$ )<sub>3</sub> produced c-PMMBL as the major product, accompanied by I-PMMBL chains (Supplementary Fig. 26). The above results show that the acidity of the LA bound to the  $\omega$ -terminus of the polymer chain impacts the ability of the  $\omega$ -terminus to attack the  $\alpha$ -terminus for cyclic polymer formation. Al( $C_6F_5$ )<sub>3</sub> is a stronger LA than B( $C_6F_5$ )<sub>3</sub> and thus provides more stabilization for the negatively charged ω-terminus, thus preventing it from attacking the  $\alpha$ -terminus and forming only the linear polymer structure. In contrast, the weaker  $-B(C_6F_5)_2$  LA sites in I and  $B(C_6F_5)_3$  in II-2B( $C_6F_5$ )<sub>3</sub> appear to provide balanced stabilization and reactivity of the negatively charged  $\omega$ -terminus for effective chain propagation and eventual cyclization. It should be noted that although both intramolecular and intermolecular LP systems produced cyclic polymer chains, their propagation and termination mechanisms are different. As revealed by MALDI-TOF MS, the slope obtained from the plot of m/z versus the number of MMBL repeat units is 112 for the polymers produced with the II-B(C<sub>6</sub>F<sub>5</sub>)<sub>3</sub> intermolecular LP compared with 224 for the polymers produced with the intramolecular trifunctional FLP. Furthermore, linear polymer chains are inevitable co-products in the polymerization with the  $II-2B(C_6F_5)_3LP$ , in which the two B acidic sites are not bound to the structure with the P site. In short, the intramolecular trifunctional FLP I is required for the selective synthesis of c-PMMBL.

Figure 6a shows the Mark–Houwink plots of  $\log[[\eta](dl\ g^{-1})]$  versus  $\log[M_w\ (g\ mol^{-1})]$  for the PMMBL samples produced with the above three LP systems. As expected, the intrinsic viscosity of the l-PMMBL produced by the II–2Al( $C_6F_5$ )<sub>3</sub> LP is higher than that of the c-PMMBL produced by the trifunctional intramolecular FLP I, which is in good agreement with the theoretical relationship of viscosity for cyclic and linear polymers ( $[\eta]_I/[\eta]_{II-Al(C_6F_5)_3}\approx 0.75$ ). As the PMMBL sample produced by II–2B( $C_6F_5$ )<sub>3</sub> is a mixture of cyclic and linear structures, its Mark–Houwink plot is located between the plots of I and II–2Al( $C_6F_5$ )<sub>3</sub>. Overall, these results demonstrate that the intramolecular, trifunctional B-P-B FLP composed of a tethered P atom and two B atoms is the necessary catalyst/initiator structure for producing c-PMMBL efficiently and selectively.

# Thermal degradation behaviour and chemical recycling of c-PMMBL

Thermal gravimetric analysis (TGA) was performed on c-PMMBL samples with various MWs and their linear counterparts with similar MWs; the results are summarized in Fig. 6b,c. Two notable differences between the l-PMMBL and c-PMMBL are readily apparent. First, the onset decomposition temperature ( $T_{\rm onset}$ ) of the l-PMMBL samples was about 300 °C, while the  $T_{\rm onset}$  of the c-PMMBL samples was ~50 °C higher. Second, the  $T_{\rm max}$  (the temperature of maximum rate of decomposition obtained from first derivative (wt% °C<sup>-1</sup>) versus temperature or derivative thermogravimetry (DTG) plots) of the c-PMMBL samples was between 391 and 395 °C, and they exhibited a

narrow thermal degradation window, as clearly shown by their sharp DTG peaks in Fig. 6b. Although the  $T_{\rm max}$  of the l-PMMBL samples also lies within a small range between 390 and 395 °C, their DTG peaks or degradation windows are much broader (Fig. 6c). However, their glass-transition temperatures ( $T_{\rm g}$ ), measured by differential scanning calorimetry, were essentially the same, spanning a narrow range between 220 and 225 °C.

To uncover the fundamental reasons for the observed significantly higher  $T_{\text{onset}}$  and narrower degradation window of c-PMMBL compared with I-PMMBL, we set out to further investigate the two topologically different PMMBL materials by in situ thermogravimetric-coupled mass spectroscopy (TGA-MS). Although full-temperature sweeps at 10 °C min<sup>-1</sup> from 30 to 600 °C (Supplementary Figs. 35–40) did not reveal any extractable insight, isothermal treatment of c-PMMBL and I-PMMBL samples at 300 °C for 60 min, followed by continued heating to 600 °C at 10 °C min<sup>-1</sup> showed significantly different thermal behaviour. Specifically, I-PMMBL experienced high total mass loss (>51%) during the isothermal heating at relatively low temperature, while c-PMMBL lost only ~10% of its mass during the same treatment (Supplementary Figs. 41-44). In addition, I-PMMBL displayed an earlier increase in the peaks at 40 and 68 AMU in the mass spectrum, which can be attributed to chain-end scissions occurring at this low temperature (300 °C). This chain-end scission pathway predominated throughout the isothermal treatment of I-PMMBL, and increasing the temperature further then led to random in-chain scissions, leading to complete degradation. The c-PMMBL sample showed a slight increase in the 40 AMU signal (against the background) during the isothermal treatment, which can perhaps be attributed to pendant group degradation. After the isothermal treatment was concluded and the temperature was ramped up, the signals of the linear sample at 40 and 68 AMU held steady for a longer temperature window than the cyclic sample, which briefly showed increases in the signals at 40 and 68 amu before the monomer (112 AMU) signal increased. We have proposed pathways for PMMBL degradation and MMBL fragmentation under MS conditions on the basis of the above data (Supplementary Fig. 45).

The greater thermal resistance of c-PMMBL compared with I-PMMBL prompted an interesting question: whether c-PMMBL could be chemically recycled as efficiently as I-PMMBL. To address this question, we followed the protocol and conditions previously reported for the depolymerization of I-PMMBL at the depolymerize a c-PMMBL sample ( $M_n = 165 \text{ kg mol}^{-1}$ , D = 1.50) under thermolysis conditions ( $400 \, ^{\circ}\text{C}$ ,  $4 \, ^{\circ}\text{h}$ ) using a short-path distillation set-up under dynamic vacuum and recovered the pure monomer MMBL in 79% yield (Supplementary Fig. 46). This yield compares well with that (76%) achieved for I-PMMBL. The non-depolymerized residue contained mostly low-MW oligomers; thus it can be expected that the use of a better designed reactor (for example, a fluidized bed reactor 7%) should increase the monomer recovery to perhaps recover the monomer near quantitatively.

## Conclusion

A covalently tethered B-P-B trifunctional, intramolecular FLP has been found to serve as both catalyst and initiator to effect the synthesis of the authentic cyclic acrylic polymer c-PMMBL composed entirely of MMBL monomer units. The detailed studies described herein have uncovered an unprecedented chain initiation reaction that generates a 16-membered macrocycle composed of two FLP catalyst molecules and two monomer molecules. This macrocycle establishes a template to direct subsequent REP, with two polymer chains growing concurrently from the two catalyst sites via pairwise monomer enchainment. Eventual cyclization occurs via nucleophilic attack of the  $\alpha$ -terminus of one chain by the  $\omega$ -terminus (nucleophilic enolate) of the other chain, resulting in ring closure to form authentic c-PMMBL with concurrent release of the FLP catalyst from the chains. The cyclic topology in c-PMMBL imparts an enhanced initial decomposition temperature

and a much narrower degradation window compared with l-PMMBL having chain ends and similar MW and  $\theta$  values, while maintaining high chemical recyclability.

#### **Online content**

Any methods, additional references, Nature Portfolio reporting summaries, source data, extended data, supplementary information, acknowledgements, peer review information; details of author contributions and competing interests; and statements of data and code availability are available at https://doi.org/10.1038/s41557-022-01097-7.

# References

- Bielawski, C. W., Benitez, D. & Grubbs, R. H. An "endless" route to cyclic polymers. Science 297, 2041–2044 (2002).
- Hong, M. & Chen, E. Y.-X. Completely recyclable biopolymers with linear and cyclic topologies via ring-opening polymerization of y-butyrolactone. *Nat. Chem.* 8, 42–49 (2016).
- 3. Haque, F. M. & Grayson, S. M. The synthesis, properties and potential applications of cyclic polymers. *Nat. Chem.* **12**, 433–444 (2020).
- 4. Endo, K. Synthesis and properties of cyclic polymers. *Adv. Polym.* Sci. **217**, 121–183 (2008).
- Zhu, J.-B., Watson, E. M., Tang, J. & Chen, E. Y.-X. A synthetic polymer system with repeatable chemical recyclability. *Science* 360, 398–403 (2018).
- Kammiyada, H., Ouchi, M. & Sawamoto, M. A study on physical properties of cyclic poly(vinyl ether)s synthesized via ring-expansion cationic polymerization. *Macromolecules* 50, 841–848 (2017).
- 7. Kricheldorf, H. R. Cyclic polymers: synthetic strategies and physical properties. *J. Polym. Sci. A* **48**, 251–284 (2010).
- 8. Ziebarth, J. D. et al. Comparison of critical adsorption points of ring polymers with linear polymers. *Macromolecules* **49**, 8780–8788 (2016).
- Gambino, T., Martínez de Ilarduya, A., Alegría, A. & Barroso-Bujans, F. Dielectric relaxations in poly(glycidyl phenyl ether): effects of microstructure and cyclic topology. *Macromolecules* 49, 1060–1069 (2016).
- Doi, Y. et al. Melt rheology of ring polystyrenes with ultrahigh purity. Macromolecules 48, 3140–3147 (2015).
- 11. Pasquino, R. et al. Viscosity of ring polymer melts. ACS Macro Lett. **2**, 874–878 (2013).
- Roland, C. D., Li, H., Abboud, K. A., Wagener, K. B. & Veige, A. S. Cyclic polymers from alkynes. *Nat. Chem.* 8, 791–796 (2016).
- Yamamoto, T. & Tezuka, Y. Cyclic polymers revealing topology effects upon self-assemblies, dynamics and responses. Soft Matter 11, 7458–7468 (2015).
- Tu, X.-Y., Liu, M.-Z. & Wei, H. Recent progress on cyclic polymers: synthesis, bioproperties, and biomedical applications. *J. Polym. Sci. A*: 54, 1447–1458 (2016).
- Williams, R. J., Dove, A. P. & O'Reilly, R. K. Self-assembly of cyclic polymers. *Polym. Chem.* 6, 2998–3008 (2015).
- Liénard, R., De Winter, J. & Coulembier, O. Cyclic polymers: advances in their synthesis, properties, and biomedical applications. J. Polym. Sci. 58, 1481–1502 (2020).
- Romio, M. et al. Topological polymer chemistry enters materials science: expanding the applicability of cyclic polymers. ACS Macro Lett. 9, 1024–1033 (2020).
- Zhang, K., Lackey, M. A., Cui, J. & Tew, G. N. Gels based on cyclic polymers. J. Am. Chem. Soc. 133, 4140–4148 (2011).
- Chen, B., Jerger, K., Fréchet, J. M. J. & Szoka, F. C. Jr The influence of polymer topology on pharmacokinetics: differences between cyclic and linear PEGylated poly(acrylic acid) comb polymers. J. Control. Release 140, 203–209 (2009).

- Wang, T.-W. & Golder, M. R. Advancing macromolecular hoop construction: recent developments in synthetic cyclic polymer chemistry. *Polym. Chem.* 12, 958–969 (2021).
- Josse, T., De Winter, J., Gerbaux, P. & Coulembier, O. Cyclic polymers by ring-closure strategies. *Angew. Chem. Int. Ed.* 55, 13944–13958 (2016).
- 22. Chang, Y. A. & Waymouth, R. M. Recent progress on the synthesis of cyclic polymers via ring-expansion strategies. *J. Polym. Sci. A* **55**, 2892–2902 (2017).
- Sarkar, S. et al. An OCO<sup>3-</sup> trianionic pincer tungsten(VI) alkylidyne: rational design of a highly active alkyne polymerization catalyst. J. Am. Chem. Soc. **134**, 4509–4512 (2012).
- Miao, Z. et al. Cyclic polyacetylene. Nat. Chem. 13, 792–799 (2021).
- Wang, T.-W., Huang, P.-R., Chow, J. L., Kaminsky, W. & Golder, M. R. A cyclic ruthenium benzylidene initiator platform enhances reactivity for ring-expansion metathesis polymerization. *J. Am. Chem.* Soc. 143, 7314–7319 (2021).
- Gonsales, S. A. et al. Highly tactic cyclic polynorbornene: stereoselective ring expansion metathesis polymerization of norbornene catalyzed by a new tethered tungsten-alkylidene catalyst. J. Am. Chem. Soc. 138, 4996–4999 (2016).
- Reisberg, S. H., Hurley, H. J., Mathers, R. T., Tanski, J. M. & Getzler, Y. D. Y. L. Lactide cyclopolymerization kinetics, X-ray structure, and solution dynamics of ('Bu-SalAmEE)Al and a cautionary tale of polymetalate formation. *Macromolecules* 46, 3273–3279 (2013).
- Piedra-Arroni, E., Ladavière, C., Amgoune, A. & Bourissou, D. Ring-opening polymerization with Zn(C<sub>6</sub>F<sub>5</sub>)<sub>2</sub>-based Lewis pairs: original and efficient approach to cyclic polyesters. *J. Am. Chem.* Soc. **135**, 13306–13309 (2013).
- Brown, H. A. & Waymouth, R. M. Zwitterionic ring-opening polymerization for the synthesis of high molecular weight cyclic polymers. Acc. Chem. Res. 46, 2585–2596 (2013).
- 30. Li, X.-Q., Wang, B., Ji, H.-Y. & Li, Y.-S. Insights into the mechanism for ring-opening polymerization of lactide catalyzed by  $Zn(C_6F_5)_2/corganic$  superbase Lewis pairs. Catal. Sci. Technol. **6**, 7763–7772 (2016).
- Asenjo-Sanz, I., Veloso, A., Miranda, J. I., Pomposo, J. A. & Barroso-Bujans, F. Zwitterionic polymerization of glycidyl monomers to cyclic polyethers with B(C<sub>6</sub>F<sub>5</sub>)<sub>3</sub>. *Polym. Chem.* 5, 6905–6908 (2014).
- Guo, L., Lahasky, S. H., Ghale, K. & Zhang, D. N-Heterocyclic carbene-mediated zwitterionic polymerization of N-substituted N-Carboxyanhydrides toward poly(α-peptoid)s: kinetic, mechanism, and architectural control. J. Am. Chem. Soc. 134, 9163–9171 (2012).
- Zhang, Y., Miyake, G. M. & Chen, E. Y.-X. Alane-based classical and frustrated Lewis pairs in polymer synthesis: rapid polymerization of MMA and naturally renewable methylene butyrolactones into high-molecular-weight polymers. *Angew. Chem. Int. Ed.* 49, 10158–10162 (2010).
- McGraw, M. L. & Chen, E. Y.-X. Lewis pair polymerization: perspective on a ten-year journey. *Macromolecules* 53, 6102–6122 (2020).
- Hong, M., Chen, J. & Chen, E. Y.-X. Polymerization of polar monomers mediated by main-group Lewis acid-base pairs. Chem. Rev. 118, 10551–10616 (2018).
- Chen, E. Y.-X. Polymerization by classical and frustrated Lewis pairs. Top. Curr. Chem. 334, 239–260 (2012).
- Wan, Y., He, J., Zhang, Y. & Chen, E. Y.-X. One-step synthesis of lignin-based triblock copolymers as high-temperature and UV-blocking thermoplastic elastomers. *Angew. Chem. Int. Ed.* (2022). https://doi.org/10.1002/anie.202114946
- 38. Stephan, D. W. Frustrated Lewis pairs: from concept to catalysis. *Acc. Chem. Res.* **48**, 306–316 (2015).

- Stephan, D. W. & Erker, G. Frustrated Lewis pair chemistry: development and perspectives. *Angew. Chem. Int. Ed.* 54, 6400–6441 (2015).
- 40. Stephan, D. W. The broadening reach of frustrated Lewis pair chemistry. Science **354**, aaf7229 (2016).
- 41. Kehr, G. & Erker, G. Frustrated Lewis pair chemistry: searching for new reactions. *Chem. Rec.* **17**, 803–815 (2017).
- 42. Jupp, A. R. & Stephan, D. W. New directions for frustrated Lewis pair chemistry. *Trends Chem.* **1**, 35–48 (2019).
- 43. Zhao, W., He, J. & Zhang, Y. Lewis pairs polymerization of polar vinyl monomers. *Sci. Bull.* **64**, 1830–1840 (2019).
- 44. Wang, Q. et al. Living polymerization of conjugated polar alkenes catalyzed by N-heterocyclic olefin-based frustrated Lewis pairs. *ACS Catal.* **8**, 3571–3578 (2018).
- Wang, H., Wang, Q., He, J. & Zhang, Y. Living polymerization of acrylamides catalysed by N-heterocyclic olefin-based Lewis pairs. *Polym. Chem.* 10, 3597–3603 (2019).
- Zhang, P., Zhou, H. & Lu, X.-B. Living and chemoselective (co) polymerization of polar divinyl monomers mediated by bulky Lewis pairs. *Macromolecules* 52, 4520–4525 (2019).
- Bai, Y., He, J. & Zhang, Y. Ultra-high-molecular-weight polymers produced by the immortal phosphine-based catalyst system.
  Angew. Chem. Int. Ed. 57, 17230–17234 (2018).
- Wang, Q., Zhao, W., He, J., Zhang, Y. & Chen, E. Y.-X. Living ring-opening polymerization of lactones by N-heterocyclic olefin/ Al(C<sub>6</sub>F<sub>5</sub>)<sub>3</sub> Lewis pairs: structures of intermediates, kinetics, and mechanism. *Macromolecules* 50, 123–136 (2017).
- Zhang, H., Nie, Y., Zhi, X., Du, H. & Yang, J. Controlled ring-opening polymerization of α-amino acid N-carboxy-anhydride by frustrated amine/borane Lewis pairs. Chem. Commun. 53, 5155–5158 (2017).
- Naumann, S., Scholten, P. B., Wilson, J. A. & Dove, A. P. Dual catalysis for selective ring-opening polymerization of lactones: evolution toward simplicity. J. Am. Chem. Soc. 137, 14439–14445 (2015).
- 51. Ji, H.-Y., Wang, B., Pan, L. & Li, Y.-S. Lewis pairs for ring-opening alternating copolymerization of cyclic anhydrides and epoxides. *Green Chem.* **20**, 641–648 (2018).
- Yang, J.-L., Wu, H.-L., Li, Y., Zhang, X.-H. & Darensbourg, D. J. Perfectly alternating and regioselective copolymerization of carbonyl sulfide and epoxides by metal-free Lewis pairs. *Angew. Chem. Int. Ed.* 56, 5774–5779 (2017).
- Zhang, D., Boopathi, S. K., Hadjichristidis, N., Gnanou, Y. & Feng, X. Metal-free alternating copolymerization of CO<sub>2</sub> with epoxides: fulfilling "green" synthesis and activity. J. Am. Chem. Soc. 138, 11117–11120 (2016).
- Zhang, J., Wang, L., Liu, S., Kang, X. & Li, Z. A Lewis pair as organocatalyst for one-pot synthesis of block copolymers from a mixture of epoxide, anhydride, and CO<sub>2</sub>. *Macromolecules* 54, 763–772 (2021).
- 55. Wang, Y. et al. Highly selective and productive synthesis of a carbon dioxide-based copolymer upon zwitterionic growth. *Macromolecules* **54**, 2178–2186 (2021).
- Liu, S. et al. Biased Lewis pairs: a general catalytic approach to ether-ester block copolymers with unlimited ordering of sequences. *Angew. Chem. Int. Ed.* 58, 15478–15487 (2019).
- Bai, Y., Wang, H., He, J. & Zhang, Y. Rapid and scalable access to sequence-controlled DHDM multiblock copolymers by FLP polymerization. *Angew. Chem. Int. Ed.* 59, 11613–11619 (2020).
- McGraw, M. L., Clarke, R. W. & Chen, E. Y.-X. Compounded sequence control in polymerization of one-pot mixtures of highly reactive acrylates by differentiating Lewis pairs. *J. Am. Chem. Soc.* 142, 5969–5973 (2020).

- McGraw, M. L., Clarke, R. W. & Chen, E. Y.-X. Synchronous control of chain length/sequence/topology for precision synthesis of cyclic block copolymers from monomer mixtures. *J. Am. Chem.* Soc. 143, 3318–3322 (2021).
- 60. Hosoi, Y., Takasu, A., Matsuoka, S. & Hayashi, M. N-Heterocyclic carbene initiated anionic polymerization of (*E,E*)-methyl sorbate and subsequent ring-closing to cyclic poly(alkyl sorbate). *J. Am. Chem. Soc.* **139**, 15005–15012 (2017).
- Oga, Y., Hosoi, Y. & Takasu, A. Synthesis of cyclic poly(methyl methacrylate) via N-heterocyclic carbene (NHC) initiated-anionic polymerization and subsequent ring-closing without need of highly dilute conditions. *Polymer* 186, 122019 (2020).
- Wang, B., Pan, L., Ma, Z. & Li, Y. Ring-opening polymerization with Lewis pairs and subsequent nucleophilic substitution: a promising strategy to well-defined polyethylene-like polyesters without transesterification. *Macromolecules* 51, 836–845 (2018).
- Wang, L.-Y. et al. Intramolecularly cooperative catalysis for copolymerization of cyclic thioanhydrides and epoxides: a dual activation strategy to well-defined polythioesters. ACS Catal. 10, 6635–6644 (2020).
- 64. Yang, G.-W., Zhang, Y.-Y., Xie, R. & Wu, G.-P. Scalable bifunctional organoboron catalysts for copolymerization of CO<sub>2</sub> and epoxides with unprecedented efficiency. *J. Am. Chem. Soc.* **142**, 12245– 12255 (2020).
- 65. Yang, G.-W., Zhang, Y.-Y., Xie, R. & Wu, G.-P. High-activity organocatalysts for polyether synthesis via intramolecular ammonium cation assisted S<sub>N</sub>2 ring-opening polymerization. *Angew. Chem. Int. Ed.* **59**, 16910–16917 (2020).
- Yang, G.-W. et al. Pinwheel-shaped tetranuclear organoboron catalysts for perfectly alternating copolymerization of CO<sub>2</sub> and epichlorohydrin. J. Am. Chem. Soc. 143, 3455–3465 (2021).
- 67. Wang, L. et al. Cooperative carbon monoxide to formyl reduction at a trifunctional PBB frustrated Lewis pair. *Chem. Commun.* **53**, 5499–5502 (2017).
- 68. Wang, L. et al. Formation of macrocyclic ring systems by carbonylation of trifunctional P/B/B frustrated Lewis pairs. *Chem. Sci.* **9**, 1544–1550 (2018).

- Zhang, Y. et al. Lewis pair polymerization by classical and frustrated Lewis pairs: acid, base and monomer scope and polymerization mechanism. *Dalton Trans.* 41, 9119–9134 (2012).
- Gowda, R. R. & Chen, E. Y.-X. Sustainable Polymers from Biomass-Derived α-Methylene-γ-Butyrolactones. in Mark, H. F. Ed. Encyclopedia of Polymer Science and Technology, 4th Ed, Vol. 8, pp. 235–271; Wiley, Hoboken, 2014.
- 71. Agarwal, S., Jin, Q. & Maji, S. Biobased polymers from plant-derived Tulipalin A. ACS Symp. Ser. **1105**, 197–212 (2012).
- Bai, Y., Wang, H., He, J., Zhang, Y. & Chen, E. Y.-X. Dual-initiating and living frustrated Lewis pairs: expeditious synthesis of biobased thermoplastic elastomers. *Nat. Commun.* 12, 4874 (2021).
- Gilsdorf, R. A., Nicki, M. A. & Chen, E. Y.-X. High chemical recyclability of vinyl lactone acrylic bioplastics. *Polym. Chem.* 11, 4942–4950 (2020).
- 74. He, J. et al. Chain propagation and termination mechanisms for polymerization of conjugated polar alkenes by [Al]-based frustrated Lewis pairs. *Macromolecules* **47**, 7765–7774 (2014).
- Xu, P. & Xu, X. Homoleptic rare-earth aryloxide based Lewis pairs for polymerization of conjugated polar alkenes. ACS Catal. 8, 198–202 (2018).
- Kaminsky, W. & Franck, J. Monomer recovery by pyrolysis of poly(methyl methacrylate) (PMMA). J. Anal. Appl. Pyrolysis 19, 311–318 (1991).

**Publisher's note** Springer Nature remains neutral with regard to jurisdictional claims in published maps and institutional affiliations.

Springer Nature or its licensor (e.g. a society or other partner) holds exclusive rights to this article under a publishing agreement with the author(s) or other rightsholder(s); author self-archiving of the accepted manuscript version of this article is solely governed by the terms of such publishing agreement and applicable law.

@ The Author(s), under exclusive licence to Springer Nature Limited 2022

## Methods

#### Materials and methods

All syntheses and manipulations of air- and moisture-sensitive materials were carried out in flame-dried Schlenk-type glassware on a dual-manifold Schlenk line or in an argon-filled glove box. NMR experiments on air-sensitive samples were conducted in Teflon valve-sealed J. Young-type NMR tubes. THF, n-pentane and hexane were refluxed over sodium-potassium alloy and distilled under nitrogen. Methylene chloride and fluorobenzene were dried with CaH2, distilled under nitrogen and then stored over molecular sieves (4 Å). [2H<sub>2</sub>]Methylene chloride and [<sup>2</sup>H<sub>6</sub>]benzene were dried over molecular sieves (4 Å). MMA and MMBL were purchased from TCI. The monomers were dried over CaH<sub>2</sub> overnight and then subjected to vacuum distillation. The dried monomers were stored in brown bottles inside a glove-box freezer at -30 °C. Vinylmagnesium bromide solution (1.0 M in THF) and ethylmagnesium bromide solution (1.0 M in THF) were purchased from Adamas. PMMA used for TGA-MS experiments was produced by group transfer polymerization with methyl trimethylsilyl dimethylketene acetal and Al( $C_6F_5$ )<sub>3</sub> ( $M_n = 44.8 \text{ kg mol}^{-1}$ ,  $\mathcal{D} = 1.18$ ). Literature procedures were followed for the preparation of the following compounds:  $B(C_6F_5)_3^{77}$ ,  $HB(C_6F_5)_2^{78}$ ,  $Mes*PCl_2$ , trifunctional intramolecular FLP I<sup>67,68</sup> and VMBL<sup>79</sup>.

# MMBL polymerization catalysed by 1A or a mixture of 1A and 1B

Polymerizations were performed in 20-ml glass reactors inside an inert glove box under N<sub>2</sub> atmosphere at ambient temperature. The monomer concentration was kept constant, while the catalyst concentration was changed according to the monomer/catalyst ratio. A predetermined amount of 1A or a mixture of 1A and 1B was first dissolved in methylene chloride. The polymerization reaction was started by addition of MMBL to the catalyst solution in methylene chloride. After a specific period of time, a 0.1 ml aliquot was removed from the reaction mixture using a pipette and quickly quenched in a 4-ml vial containing 0.6 ml of undried 'wet' CDCl<sub>3</sub> stabilized by 250 ppm BHT(butylated hydroxytoluene). The quenched aliquots were later analysed by <sup>1</sup>H NMR spectroscopy to determine the monomer conversion. After stirring the polymerization mixture for the stated reaction time, the reactor was removed from the glove box and the reaction quenched by the addition of 5 ml hexane. The quenched reaction mixture was isolated by filtration and dried in a vacuum oven at room temperature to a constant weight.

# MMBL polymerization catalysed by intermolecular LP $II-2B(C_6F_5)_3$ or $II-2AI(C_6F_5)_3$

All polymerizations were performed in 20-ml glass reactors inside an inert glove box under N<sub>2</sub> atmosphere at ambient temperature. The monomer concentration was kept constant, while the catalyst concentration was changed according to the monomer/catalyst ratio. A predetermined amount of LA B( $C_6F_5$ )<sub>3</sub> or Al( $C_6F_5$ )<sub>3</sub> (in the form of the adduct Al( $C_6F_5$ )<sub>3</sub>·MMBL) was first dissolved in monomer and methylene chloride. The polymerization reaction was started by the rapid addition of a solution of **II** in methylene chloride by pipette to the above mixture under vigorous stirring. After a specific period of time, a 0.1 ml aliquot was removed from the reaction mixture using a pipette and quickly quenched in a 4-ml vial containing 0.6 ml of undried 'wet' CDCl<sub>3</sub> stabilized by 250 ppm BHT. The quenched aliquots were later analysed by <sup>1</sup>H NMR spectroscopy to determine the monomer conversion. After stirring the polymerization mixture for the stated reaction time, the reactor was removed from the glove box and the reaction was quenched by the addition of 5 ml hexane. The quenched reaction mixture was isolated by filtration and dried in a vacuum oven at room temperature to a constant weight.

## Characterizations

NMR spectra were recorded on a Bruker Avance II 500 spectrometer (<sup>1</sup>H, 500 MHz; <sup>13</sup>C, 126 MHz; <sup>19</sup>F, 471 MHz; <sup>31</sup>P, 202 MHz) or a

Zhongke-Niujin 400 ( $^{1}$ H, 400 MHz) spectrometer at room temperature. The  $^{1}$ H and  $^{13}$ C chemical shifts are referenced to internal solvent resonances and reported as parts per million relative to SiMe<sub>4</sub>, and the  $^{19}$ F chemical shifts are referenced to external CFCl<sub>3</sub>. Single-crystal X-ray diffraction analysis was performed on a Bruker APEX-II CCD diffractometer.

The isolated low-MW oligomeric samples were analysed by MALDI-TOF MS on a Bruker Autoflex speed TOF/TOF mass spectrometer in linear, positive ion, reflector mode using a 355 nm Nd:YAG laser and an accelerating voltage of 25 kV. A thin layer of 1% CF $_3$ COONa or CF $_3$ COOK solution was first deposited on the target plate, followed by 0.6  $\mu$ l of both polymer samples and the matrix trans-2-[3-(4-tert-butylphenyl)-2-methyl-2-propenylidene]malonitrile (20 mg ml  $^{-1}$  in THF). External calibration was carried out using a peptide calibration mixture (four to six peptides) at a spot adjacent to the sample. The raw data were processed using the FlexAnalysis software.

The low-MW PMMBL samples were prepared for MALDI-TOF MS analysis as follows:

- 1) Synthesis of low-MW PMMBL samples with FLP I: 0.0100 g FLP I (0.0098 mmol, 1 equiv.) was dissolved in 1 ml CH<sub>2</sub>Cl<sub>2</sub>. Next, 10 μl MMBL was dissolved in 2 ml CH<sub>2</sub>Cl<sub>2</sub> and 1 ml of this solution containing ~5 μl MMBL (0.0468 mmol, ~4.8 equiv.) was removed and injected into the above-mentioned FLP I solution to initiate polymerization. After 3 h, the polymers were isolated and analysed by MALDI-TOF MS.
- (2) Synthesis of low-MW PMMBL with a mixture of 1A and 1B: 0.0054 g of a mixture of 1A and 1B (0.00476 mmol, 1 equiv.) was dissolved in 1 ml CH<sub>2</sub>Cl<sub>2</sub>. Then 20 μl MMBL (0.1837 mmol, -3 equiv.) was added to the above solution to initiate polymerization. After 1 h, the polymers were isolated and analysed by MALDI-TOF MS.
- (3) Synthesis of low-MW PMMBL with LB II  $-2B(C_6F_5)_3$ , II  $-2Al(C_6F_5)_3$  or IAP $-2Al(C_6F_5)_3$ : 0.0120 g  $B(C_6F_5)_3$  (0.0234 mmol, 2 equiv.) or 0.0135 g Al $(C_6F_5)_3$ ·0.5toluene (0.0234 mmol, 2 equiv.) and 25  $\mu$ l MMBL (0.234 mmol, 20 equiv.) were premixed in 1.5 ml CH<sub>2</sub>Cl<sub>2</sub>. Then 0.0039 g LB II (0.0117 mmol,1 equiv.) or 0.0044 g LB IAP (0.0117 mmol,1 equiv.) was dissolved in 500  $\mu$ l CH<sub>2</sub>Cl<sub>2</sub>, then added to the above solution to initiate polymerization. After 1 h, the polymers were isolated and analysed by MALDI-TOF MS.

Polymer  $M_{\rm w}$  and molecular weight distributions ( $\mathcal{D}=M_{\rm w}/M_{\rm n}$ ) were measured by GPC coupled to a Wyatt DAWAN 8+ light scattering detector at 35 °C and a flow rate of 1.0 ml min<sup>-1</sup>, with N,N-dimethylformamide (DMF; HPLC grade, containing 50 mmol l<sup>-1</sup> LiBr) as eluent on a Waters 1515 HPLC pump (solvent delivery system) equipped with a Waters 4.6 mm × 30 mm guard column and three Waters columns (WAT054466, WAT044226 and WAT044223, Polymer Laboratories, linear range of MW = 500 to 4 × 10<sup>6</sup>). The data for the Mark–Houwink plots were obtained from polymers on a Waters 1515 instrument equipped with a triple detector (Wyatt DAWAN 8+ light scattering, Waters 2414 refractive index and Wyatt ViscoStar II viscometer) at 35 °C and a flow rate of 1.0 ml min<sup>-1</sup>, with DMF as the eluent. The differential refractive index increment  $(d_{\rm n}/d_{\rm c})$  value of 0.0844 ml g<sup>-1</sup> was used for PMMBL.

TGA analysis was performed on a Q50 TGA analyser (TA Instruments) to determine the decomposition temperatures ( $T_{\rm d,5\%}$ ) and the temperature of maximum rate of decomposition ( $T_{\rm max}$ ) of the polymers.  $T_{\rm d,5\%}$  is defined as the temperature at which 5% weight loss occurs.  $T_{\rm max}$  values were obtained from derivative (wt% °C<sup>-1</sup>) versus temperature (°C) plots by selecting the peak values. Between 3.5 and 10 mg of polymer was heated from room temperature to 500 °C at 10 °C min<sup>-1</sup> while the mass of the sample was continuously measured. Differential scanning calorimetry was performed on a Q20 instrument (TA Instruments) to obtain the glass transition temperature ( $T_{\rm e}$ ). Between 3 and 10 mg of polymer was weighed into an aluminium

pan and sealed with an aluminium lid. The samples were then heated from room temperature to  $250\,^{\circ}\text{C}$  at  $10-20\,^{\circ}\text{C}$  min $^{-1}$  and then cooled to  $150\,^{\circ}\text{C}$  to remove the thermal history before being reheated to  $250\,^{\circ}\text{C}$ . During this time, the thermal response was measured relative to a reference pan.

TGA-MS experiments were performed with a TGA-55 thermogravimetric analyser (TA Instruments) fitted with an evolved gas analysis furnace (TA Instruments). The analyser was coupled to a Cirrus 3 electron ionization mass spectrometer (MKS Instruments). The TGA data were processed using TRIOS software (TA Instruments, v5.1.1.46572), and the MS data were processed using both TRIOS and ProcessEye Professional software (MKS Instruments, v5.83.20111.1). In a standard TGA-MS experiment, polymer samples of between 3 and 5 mg were heated from 30 to 600 °C at 10 °C min<sup>-1</sup> with nitrogen flow rates through the balance and furnace of 10 and 90 ml min<sup>-1</sup>, respectively, while the sample mass was continuously measured and MS data were collected.  $T_{d.5\%}$  and  $T_{max}$  values were obtained from derivative (wt% °C<sup>-1</sup>) versus temperature plots by selecting the point of the weight percentage versus temperature (°C) corresponding to 95 wt% of sample remaining (for  $T_{d.5\%}$ ) and the maximum point (for  $T_{\text{max}}$ ). The mass spectra were captured at the maximum signal of the decomposition products for all samples. In the isothermal experiments, polymer samples of between 3 and 5 mg were heated from 30 to 300 °C at 10 °C min<sup>-1</sup> with nitrogen flow rates through the balance and furnace of 10 and 90 ml min<sup>-1</sup>, respectively, allowed to equilibrate and then held at 300 °C for 1 h. The samples were then heated to 600 °C at 10 °C min<sup>-1</sup>. MS data were collected continuously throughout the experiments. The mass spectra for the isothermal experiments were collected at precisely 41 min and 40 s during the isothermal stage of each experiment.

# Data availability

Full experimental details and the data supporting the findings of this study are available within the article and its Supplementary Information. Source data are provided with this paper.

#### References

 Kuprat, M., Lehmann, M., Schulz, A. & Villinger, A. Synthesis of pentafluorophenyl silver by means of Lewis acid catalysis: structure of silver solvent complexes. *Organometallics* 29, 1421–1427 (2010).

- Parks, D. J., Piers, W. E. & Yap, G. P. A. Synthesis, properties, and hydroboration activity of the highly electrophilic borane bis(pentafluorophenyl)borane, HB(C<sub>6</sub>F<sub>5</sub>)<sub>2</sub>. Organometallics 17, 5492–5503 (1998).
- Sudhakar, G., Satish, K. & Raghavaiah, J. Total synthesis and absolute configuration of curvularides A–E. J. Org. Chem. 77, 10010–10020 (2012).

# **Acknowledgements**

This work was supported by the National Natural Science Foundation of China (grant nos. 22071077 and 21871107) to Y.Z. and the US National Science Foundation (NSF-1904962) to E.Y.-X.C. The funders had no role in study design, data collection and analysis, decision to publish or preparation of the manuscript.

# **Author contributions**

Y.Z. and Y.S. conceived the idea and designed the experiments. Y.S. and R.A.G performed the experiments and characterizations. Y.S., J.H., Y.Z. and E.Y.-X.C. analysed the data, wrote parts of the manuscript and provided input. Y.Z. directed the project.

# **Competing interests**

Y.Z., Y.S. and J.H. are named inventors on a Chinese patent application (number 202111184369.9) submitted by Jilin University that covers the preparation and characterization of cyclic PMMBL. The other authors (R.A.G. and E. Y.-X.C.) declare no competing interests.

# **Additional information**

**Supplementary information** The online version contains supplementary material available at https://doi.org/10.1038/s41557-022-01097-7.

**Correspondence and requests for materials** should be addressed to Yuetao Zhang.

**Peer review information** *Nature Chemistry* thanks Kai Guo and the other, anonymous, reviewer(s) for their contribution to the peer review of this work.

**Reprints and permissions information** is available at www.nature.com/reprints.